Co-evolution of Eukaryotic-like Vps4 and ESCRT-III Subunits in the Asgard Archaea

Zhongyi Lu[a,b], Ting Fu[c,h], Tianyi Li[d,e], Yang Liu[a], Siyu Zhang[a,f], Jinquan Li[a], Junbiao Dai[d,e], Eugene V Koonin[g], Guohui Li[c], Huiying Chu[c#], Meng Li[a#].

[a]Shenzhen Key Laboratory of Marine Microbiome Engineering, Institute for Advanced Study, Shenzhen University, Shenzhen 518060, China

[b]Key Laboratory of Optoelectronic Devices and Systems of Ministry of Education and Guangdong Province, College of Optoelectronic Engineering, Shenzhen University, Shenzhen 518060, China

[c]Laboratory of Molecular Modeling and Design, State Key Laboratory of Molecular Reaction Dynamics, Dalian Institute of Chemical Physics, Chinese Academy of Sciences, Dalian 116023, China

[d]Guangdong Provincial Key Laboratory of Synthetic Genomics, CAS Key Laboratory of Quantitative Engineering Biology and Shenzhen Key Laboratory of Synthetic Genomics, Shenzhen Institute of Synthetic Biology, Shenzhen Institutes of Advanced Technology, Chinese Academy of Sciences, Shenzhen 518055, China

[e]Key Laboratory of Industrial Biocatalysis (Ministry of Education) and Cent

er for Synthetic and Systems Biology, School of Life Sciences, Tsinghua University, Beijing 100084, China

[f]College of Life Sciences and Oceanography, Shenzhen University, Shenzhen 518060, China

[g]National Center for Biotechnology Information, National Library of Medicine, Bethesda, MD 20894, USA

[h]Pharmacy Department of Affiliated Zhongshan Hospital of Dalian University, Dalian 116001, China

Running Head: Vps4 and ESCRT-III in Asgard archaea

[#]Address correspondence to Meng Li, limeng848@szu.edu.cn and Huiying Chu, chuhy2009@dicp.ac.cn.

Zhongyi Lu and Ting Fu contributed equally to this work. Author order was determined in order of increasing seniority.

ABSTRACT (246 words)

The emergence of the endomembrane system is a key step in the evolution of cellular complexity during eukaryogenesis. The Endosomal Sorting Complex Required for Transport (ESCRT) machinery is essential and required for the endomembrane system functions in eukaryotic cells. Recently, genes encoding eukaryote-like ESCRT protein components have been identified in the genomes of Asgard archaea, a newly proposed archaeal superphylum that is thought to include the closest extant prokaryotic relatives of eukaryotes. However, structural and functional features of Asgard ESCRT remain uncharacterized. Here we show that Vps4, Vps2/24/46, and Vps20/32/60, the core functional components of the Asgard ESCRT, co-evolved eukaryote-like structural and functional features. Phylogenetic analysis shows that Asgard Vps4, Vps2/24/46, and Vps20/32/60 are closely related to their eukaryotic counterparts. Molecular dynamic simulation and biochemical assays indicate that Asgard Vps4 contains a eukaryote-like Microtubule Interacting and Transport (MIT) domain that binds the distinct type-1 MIT Interacting Motif and type-2 MIT Interacting Motif in Vps2/24/46, and Vps20/32/60, respectively. The Asgard Vps4 partly, but much more efficiently than homologs from other archaea, complements the *vps4* null mutant of *Saccharomyces cerevisiae*, further

supporting the functional similarity between the membrane remodeling machineries of Asgard archaea and eukaryotes. Thus, this work provides evidence that the ESCRT complexes from Asgard archaea and eukaryotes are evolutionarily related and functionally similar. Thus, despite the apparent absence of endomembranes in Asgard archaea, the eukaryotic ESCRT seems to have been directly inherited from an Asgard ancestor, to become a key component of the emerging endomembrane system.

IMPORTANCE (105 words)

The discovery of Asgard archaea has changed the exiting ideas on the origins of Eukaryotes. Researchers propose that eukaryotic cells evolve from Asgard archaea. This hypothesis partly stems from the presence of multiple eukaryotic signature proteins in Asgard archaea, including homologues of ESCRT proteins that are essential components of the endomembrane system in eukaryotes. However, structural and functional features of Asgard ESCRT remain unknown. Our study provides evidence that Asgard ESCRT is functionally comparable to the eukaryotic counterparts suggesting that, despite the apparent absence of endomembranes in archaea, eukaryotic ESCRT was inherited from an Asgard archaeal ancestor, alongside the emergence of endomembrane system during eukaryogenesis.

76 **Keywords**: Endomembrane system, Asgard archaea, ESCRT,

77 Eukaryogenesis, Evolution.

78

INTRODUCTION (4595 words)

Eukaryogenesis is a major, long-standing puzzle in evolutionary biology because the specifics of the evolutionary process leading to the eukaryotic cellular complexity are far from being clear. One of the key distinctions of eukaryotic cells from the cells of prokaryotes is the presence in the former of the sophisticated endomembrane system. Undoubtedly, the emergence of the endomembrane system was a milestone event in eukaryogenesis because it is a pre-requisite of the intracellular compartmentalization which is a hallmark of eukaryotic cells (1). The Endosomal Sorting Complex Required for Transport (ESCRT) machinery is an essential component of the eukaryotic endomembrane system that, as such, has been thought to be restricted to eukaryotic cells (2). For instance, *Saccharomyces cerevisiae* ESCRT consists of five main subcomplexes: ESCRT-0, -I, -II, -III, and Vps4 (3-5). Of these, the Vps4 and ESCRT-III subunits are central players in ESCRT function that mediates remodelling and scission of endomembranes (6, 7). The ESCRT-III subunits can be further divided into two classes, termed Vps2/24/46 and Vps20/32/60, and both participate in either directly or indirectly forming membrane-bound polymeric assemblies that sever membrane necks (8). On the other hand, Vps4, an ATPase, promotes ATP-dependent disassembly of the ESCRT-III

polymers, thus ensuring the ESCRT-III subunits turnover. Several studies have shown that the N-terminal Microtubule Interacting and Transport (MIT) domain of Vps4 recognizes and interacts with the type-1 MIT Interacting Motif (MIM1) that is present in the Vps2/24/46 class ESCRT-III subunits and type-2 MIT Interacting Motif (MIM2) present in the Vps20/32/60 subunits. These recognition models are essential for the biological function of ESCRT-III and Vps4 (9-11).

The cell division (Cdv) systems discovered in some archaeal orders, such as Sulfolobales and Desulfurococcales within the TACK (Thaumarchaeota, Aigarchaeota, Crenarchaeota, and Korarchaeota) superphylum include a homolog of eukaryotic Vps4 (CdvC) and several homologs of eukaryotic ESCRT-III subunits (CdvBs) (12, 13). Given these homologies and because in eukaryotes, the MIT-MIM2 interactions occurred between CdvC and CdvB (12, 14, 15), the creanarchaeal Cdv system has been proposed to be the evolutionary ancestor of eukaryotic ESCRT (16). However, this evolutionary relationship remains uncertain. One reason for the uncertainty is that CdvBs lack the well-characterized MIM1, and the absence of the MIT-MIM1 interaction is likely to reflect major functional differences between crenarchaeal Cdv and eukaryotic ESCRT (12, 17). Such differences might indicate that, although the two systems consist of

119 homologous subunits, the Cdv system is not the direct ancestor of eukaryotic
120 ESCRT.

121 The recently discovered Asgard archaea (including Lokiarchaeota,
122 Thorarchaeota, Heimdallarchaeota, Odinarchaeota, and Helarchaeota) have
123 been proposed to include the closest archaeal relatives of eukaryotes. This
124 proposition stems, partly, from the findings that the Asgard genomes encode
125 a broad repertoire of Eukaryotic Signature Proteins (ESPs) that are far more
126 prevalent in Asgard than they are in other archaea (18-21). Among these
127 ESPs are highly conserved homologs of eukaryotic ESCRT-I, -II, -III, and
128 Vps4. Notably, the presence of these proteins in Asgard archaea that was
129 originally demonstrated on metagenomics assemblies has been confirmed by
130 analysis of the first closed Asgard genome, ruling out the possibility of a
131 eukaryotic contamination (12, 18, 19, 22).

132 Here, we explore the phylogenetic relationships among the ESCRT-III
133 components, reconstitute and biochemically characterize the Asgard Vps4,
134 and test its potential biological function in the heterologous *S. cerevisiae*
135 endomembrane system. The combined phylogenetic, genetic and
136 biochemical analyses reveal close relationships between the ESCRT-III
137 subunits and Vps4 of Asgard archaea and eukaryotes, to the exclusion of
138 other archaea.

RESULTS

Eukaryotic-like ESCRT-III subunits and Vps4 in Asgard archaea

Given that the ESCRT-III subunits are tightly linked to the functional complexity of ESCRT (12), we first performed a detailed sequence comparison and phylogenetic analysis of the Vps2/24/46 and Vps20/32/60 as well as the Vps4 ATPase from Asgard archaea based on the available genomic data(18, 19). In the unrooted maximum-likelihood phylogenetic tree Vps2/24/46 and Vps20/32/60, the Asgard proteins form a cluster with eukaryotic homologs that is separated from the archaeal (TACK) CdvB cluster by a long branch (Fig. 1A, Fig. S1 and Table S1), supporting the notion that Asgard archaea possess "eukaryote-like" ESCRT-III subunits. All the Asgard Vps20/32/60 proteins form a strongly supported clade with the eukaryotic Vps20/32/60 which is compatible with a direct ancestral relationship. The Asgard Vps2/24/46 proteins formed three clades one of which (Odinarchaeota, Lokiarchaeota, and Thorarchaeota) clustered with the eukaryotic homologs whereas the remaining two (Heimdallarchaeota) placed near the root of the Asgard-eukaryote branch (Fig. 1A). This tree topology is likely to result from acceleration of evolution in Heimdallarchaeota.

In addition to the phylogenetic results, we found that the Asgard

Vps2/24/46 contained leucine-rich motifs located in the C-terminal helix and resembling the C-terminal MIM1 that are conserved in eukaryotes although some leucine residues were substituted by isoleucine in the Asgard homologs (Fig. 1B) (9). The C-terminal regions of the Asgard Vps20/32/60 contain proline-rich motifs that resemble MIM2 although do not fully conform to the MIM2 consensus in eukaryotes and TACK archaea (10, 11). Taken together, the results of phylogenetic analysis and motif search for ESCRT-III subunits not only demonstrate the Asgard-eukaryote affinity but also show that the ancestors of the Vps2/24/46 and Vps20/32/60 groups have already diverged in Asgard archaea, antedating eukaryogenesis.

It appears likely that Vps4 structurally and functionally co-evolved with ESCRT-III subunits in Asgard archaea. To explore the evolution of Vps4, an unrooted maximum-likelihood phylogenetic tree was constructed for the group of ATPases including CdvC from the TACK superphylum, Asgard Vps4, and the so called eukaryotic "meiotic clade" comprised of Vps4, Katanin 60, and Spastin (23). As in the ESCRT-III subunit tree, the Asgard Vps4 formed a branch with the eukaryotic homolog that was separated by a long, strongly supported branch from the archaeal CdvC branch (Fig. 2A and Fig. S2). The Asgard Vps4 did not form a single clade, but rather four clades, all of which were located close to the root of the Asgard-eukaryote

179 branch.

180 Despite their high divergence demonstrated by the lack of monophyly
181 in the phylogenetic tree (Fig. 2A and Fig. S2), all Asgard Vps4 contain the
182 eukaryotic-like "arginine collar" that consists of three conserved arginine
183 residues (Fig. S3A). In eukaryotes, this motif is located in the pore loop 2
184 of Vps4 and is involved in the ESCRT-III filaments translocation to the
185 central pore of the Vps4 hexamer for disassembly (Fig. S3B) (24, 25).

186 Because Vps4 recognizes ESCRT-III subunits via the MIT domain, we
187 specifically analyzed the phylogeny of the MIT domains of the Vps4
188 proteins from Asgard archaea, eukaryotes, and TACK archaea. The tree
189 demonstrates a clear affiliation of Asgard with eukaryotes that, in this case,
190 form a clade with one of the MIT domain from Heimdallarchaeota (Fig. 2B
191 and Fig. S4). Affiliation with Heimdallarchaeota has been previously
192 observed for many Asgard genes(19, 26, 27).

193 To further structurally characterize MIT domain in Asgard Vps4, we
194 constructed stable models of full length Vps4 from
195 Heimdallarchaeota_LC_3, Odinarchaeota_LCB_4, Thorarchaeota_AB_25,
196 and Lokiarchaeum_GC14_75 using homology modeling and molecular
197 dynamics simulation, and compared these with the *S. cerevisiae* Vps4
198 structure. As a control for the Asgard Vps4, we include CdvC from

*Sulfolobus solfataricus*_P2 (cluster I in Fig. 2A) and Bathyarchaeota (cluster II in Fig. 2A). All MIT domains of Asgard Vps4 and TACK CdvC adopted a three-helix bundle structure that is closely similar to the *S. cerevisiae* MIT domain structure although the helices in both the Asgard and TACK structures are somewhat shorter than in the *S. cerevisiae* structure (Fig. 2Bb and Fig. S5).

Taken together, the above data suggest that the evolution of Asgard Vps4, especially their MIT domain, was accompanied by the functional divergence of the ESCRT-III subunits. Thus, although the Asgard Vps4 proteins are highly diverged, the results of sequence comparison, phylogenetic analysis and structural modeling are compatible with coevolution of Vps4 with ESCRT-III subunits and an ancestral relationship between the membrane remodeling machineries of Asgard and eukaryotes. Furthermore, it can be predicted that Asgard Vps2/24/46 and Vps20/32/60 form ESCRT-III-like filaments similar to those in eukaryotes.

Interactions between Asgard Vps4 and ESCRT-III subunits

As previously described, unlike the CdvBs, Asgard Vps2/24/46 and Vps20/32/60 share the same eukaryotic ESCRT-III secondary structure, and these organizations are probably responsible for their ability bind to Vps4

like their eukaryotic counterparts(12). The isothermal titration calorimetry (ITC) was adopted to verify that the MIT domain of Asgard Vps4 bind to Vps2/24/46 and Vps20/32/60, respectively (Fig. S6). To characterize the interactions between Asgard Vps4 and ESCRT-III subunits, the respective binding free energies were estimated by MM-GBSA calculations (Table S2A) (28, 29). The binding free energies of Vps4-Vps2/24/46 in Heimdall_LC_3, Odin_LCB_4, Thor_AB_25, and Loki_GC14_75 were calculated as -39.02, -61.85, -71.81, -72.24 kcal/mol, respectively. All these values, although compatible with stable binding, are lower than the binding free energy of Vps4-Vps2 (-82.98 kcal/mol) in *S. cerevisiae*, suggesting that the affinity of Asgard Vps4 for Vps2/24/46 is weaker than that of *S. cerevisiae* Vps4 for Vps2. The binding free energies for Asgard Vps4-Vps20/32/60 differed to a greater degree indicating variation in the affinities (Table S2B). The Thor_AB_25 value of -119.97 kcal/mol was substantially greater than the binding free energy of the Vps4-Vps20 interaction in *S. cerevisiae* (-88.30 kcal/mol), the values for Heimdall_LC_3 (-81.43 kcal/mol) and Loki_GC14_75 (-88.89 kcal/mol) comparable to those for *S. cerevisiae*, and that for Odin_LCB_4 (-49.53 kcal/mol) much lower than in *S. cerevisiae*.

We further analyzed the structural basis for the MIT domain of Asgard

Vps4 binding to the putative MIM1 and MIM2 of Vps2/24/46 and Vps20/32/60, respectively, by using MM-GBSA calculations(28). The key amino acids that contribute to the Vps4 MIT domain binding to the Vps2/24/46 MIM1 in Heimdall_LC_3, Odin_LCB_4, and Thor_AB_25 are mainly located in Helix 2 and Helix 3 of the MIT domain similar to the location of MIM1-interacting residues in *S. cerevisiae* Vps4 (Fig. 3A and Table S3). These findings are consistent the MIM1 peptide biding at the interface between Helix 2 and Helix 3 of the MIT domain as observed in eukaryotes (10, 30). In Loki_GC14_75, the key amino acid residues are located in Helix 1 and Helix 2, suggesting a distinct interaction mode.

The key residues involved in the MIT-Vps20/32/60 interactions are spread among Helix 1, Helix 2, and Helix 3, in positions closely similar to those involved in the MIT-Vps20 interactions in *S. cerevisiae* (Fig. 3B and Table S4). Thus, the MIM2 peptide is predicted to bind the grooves formed by the three-helix bundle rather than Helix 1 and Helix 3 only as also observed for the eukaryotic ESCRT-III (10, 11). Taken together, these findings indicate that the interactions of the Asgard Vps4 MIT domain with the MIM1 (in Vps2/24/46) and MIM2 (in Vps20/32/60) motifs closely resemble the corresponding interactions in eukaryotes.

Asgard Vps4 phenotypically complements *vps4* null mutation in *S. cerevisiae*

We further sought to determine whether the Asgard and eukaryotic Vps4 ATPases were functionally interchangeable. To this end, Heimdall_LC_3, Odin_LCB_4, Thor_AB_25 and Loki_GC14_75 were tested for the ability to complement the *S. cerevisiae vps4* null mutation. As a control for the Asgard Vps4, we performed the complementation assays with CdvC from *S. solfataricus*_P2 and Bathyarchaeota. Briefly, we re-codon-optimized the coding sequences of Asgard Vps4 and TACK CdvC for expression in *S. cerevisiae*, and, respectively, assembled the coding sequences into transcription units of pPOT-RFP vector that contains a native promoter region of *S. cerevisiae* BY4741 *vps4* (a 500 bp DNA sequence region upstream from the ATG start codon of this gene) and a *S. cerevisiae* Cytochrome c isoform 1 (CYC1) terminator using the YeastFab Assembly method.(31) The assembly products were transformed into *S. cerevisiae vps4Δ* by the LiAc/PEG method(32). As previously described, in *S. cerevisiae*, *vps4* null mutation resulted in temperature-sensitive growth defect, causing growth arrest at 39 °C (33, 34). We found that the Asgard Vps4 could slightly suppress the growth defect of *vps4Δ* at 39 °C (Fig. 4A). Remarkably, however, after incubation at 39 °C for 96 h, the growth of

279 *vps4Δ* bearing Asgard Vps4 showed substantial, although variable,
280 restoration at 30 °C, in a sharp contrast with *vps4Δ* for which no restoration
281 was observed (Fig. 4A). Nevertheless, both CdvCs showed only minimal
282 growth restoration of *vps4Δ* at 39 °C and a limited enhancement of viability
283 at 30° C; complemetation with these proteins was subtantially less eifficient
284 than that observed with their Asgard counterparts. Furthermore, the *S.*
285 *cerevisiae* Vps4, Asgard Vps4, and CdvCs were re-codon-optimized,
286 synthesized, and respectively, cloned into a pCold-TF vector (Takara Bio Co
287 Ltd., Japan). After expression in *Escherichia coli* BL21, proteins were
288 purified by Mag-Beads His-Tag Protein Purification Kit (BBI Co., Ltd,
289 China). The biochemical experiments *in vitro* show that these purified
290 proteins are active ATPases both at 30 °C and 39 °C (Fig. 4B). This
291 observation eliminates the possibility that the poor complement result of
292 CdvCs was due to the lack of ATPases activity at 39 °C, and is compatible
293 with the involvement of the ATPase activity of Asgard Vps4 in sustaining
294 the viability of the *S. cerevisiae vps4Δ* mutant under non-permissive
295 conditions.

296 As previously described, *vps4* null mutation could induce an formation
297 of an aberrant prevacuolar compartment adjacent to the vacuoles, known as
298 class E compartment, due to the block of intracellular protein trafficking (3,

30, 33). To further demonstrate that Asgard Vps4 is functionally analogous to its eukaryotic counterpart, we observed the vacuoles in the *S. cerevisiae* cells bearing Asgard Vps4. As expected, the characterized class E compartment vacuolar morphology was clearly observed in the *S. cerevisiae* *vps4Δ* cells, and this defect was almost completely rescued by *S. cerevisiae* Vps4 (Fig. 4C). We found that the Vps4 of Heimdall_LC_3, Odin_LCB_4, Thor_AB_25, and Loki_GC14_75 also partially complemented the aberrant vacuoles in the *vps4* null mutant, with the reduction of class E compartment of about 80% of that observed with the native *S. cerevisiae* Vps4 (Fig. 4C). However, the enlarged vacuoles induced in *vps4Δ* strain were not markedly eliminated by the Asgard Vps4. Taken together, these findings show that the Asgard Vps4 are functionally more similar to the eukaryotic homologs than homologs from other archaea.

DISCUSSION

In this work, we combined computational approaches, including sequence comparison, phylogenetic analysis and structural modeling, with genetic and biochemical experiments to investigate the evolutionary and functional relationships between the ESCRT-III machineries of Asgard archaea and eukaryotes. Phylogenetic analyses of both the ESCRT-III

subunits and Vps4 ATPase show a clear affinity between Asgard archaea and eukaryotes, to the exclusion of the other archaea. Moreover, the divergence of the two groups of ESCRT-III subunits already occurred in Asgard archaea.

The results of amino acid sequence analysis and structural modeling are best compatible with the coevolution of Vps4 with the ESCRT-III subunits. In particular, the interaction between the MIT domain of Vps4 and the MIM1- and MIM2-like of the ESCRT-III subunits appears to have evolved already in Asgard archaea.

The findings of the computational analysis are complemented by our experimental results. In particular, we show that Asgard Vps4 is capable of complementing the *S. cerevisiae* vps4 null mutant much more efficiently than homologs from Crenarchaeota and Bathyarchaeota. This enhanced functionality might be underpinned by the evolution of distinct, "eukaryote-like" structural features, such as the arginine collar that is involved in the disassembly of ESCRT-III polymers.

Taken together, all these findings are compatible with the direct origin of the eukaryotic ESCRT machinery from the Asgard ancestor. In a broader evolutionary context, the ESCRT complex likely evolved in the common ancestor of the TACK and Asgard superphyla whereas its further elaboration

339 occurred in the Asgard lineage. The key event apparently was the
340 duplication of CdvB that seems to combine features of Vps2/24/46 and
341 Vps20/32/60 (12), with subsequent functional diversification of the subunits
342 and coevolution with Vps4.

343 An intriguing outstanding question is the function of the ESCRT
344 machinery in the Asgard archaea. There is no indication that these (or any
345 other) archaea possess intracellular membranes (22), so the ECRT-III
346 proteins and Vps4 are likely to be involved in cell division as demonstrated
347 for the Cdv proteins of Crenarchaeota. However, the specialization of the
348 ESCRT-III subunits might provide for the formation of eukaryotic-like
349 filaments that could be involved not only in the inside-out fission to produce
350 membrane vesicles that have been observed in the MK-D1 strain, but also
351 the outside-in fission that allows the Asgard archaea to engulf their bacterial
352 metabolic partners. The latter capability is critical for the 'Entangle-Engulf-
353 Enslave model' of eukaryogenesis (22). Further molecular and cell
354 biological study of the Asgard membrane remodeling apparatus, even if
355 challenging due to the recalcitrance of these organisms to growth in culture,
356 should shed light on the origin of the eukaryotic endomembrane system, one
357 of the key aspects of eukaryogenesis.

358

MATERIALS and METHODS

Bioinformatics analysis

All the protein sequences were obtained either by NCBI accession number or by BLAST search(35) the non-redundant protein sequences against local Nr database. The protein sequences were aligned using MUSCLE (V3.8.1551)(36), trimmed with TrimAl (V1.4)(37) before construction of phylogenetic trees using IQ-Tree (V1.6.5)(38). The indicated functional domains of proteins were analyzed by Interpro (https://www.ebi.ac.uk/interpro/) and NCBI's conserved domain database.

Homology modeling and docking study

We searched the Vps4, Vps2/24/46, and Vps20/32/60 sequences belonging to *S. cerevisiae*, Lokiarchaeum_GC14_75, Thorarchaeota_AB_25, Heimdallarchaeota_LC_3, and Odinarchaeota_LCB_4 from NCBI database and CdvC sequences belonging to to *Sulfolobus solfataricus*_P2, and Bathyarchaeota (http://www.ncbi.nlm.nih.gov, accession number: KZV07689.1, P36108.2, NP_013794.1; KKK42121.1, KKK42122.1, KKK44605.1; OLS30569.1, OLS30568.1, OLS30800.1; OLS27542.1, OLS27541.1, OLS27540.1; OLS18192.1, OLS18193.1, OLS18194.1, AAK41192.1, WP_119819537.1, respectively) to build homology model. The Cryo-EM structure of Vps4 (E233Q) hexamer belonging to *S. cerevisiae*

was obtained from the Protein Data Bank (PDB code: 5XMI)(39), and the subunit B was choosen for modeling template and the missing residues (1-118) were built at the I-TASSER server (http://zhanglab.ccmb.med.umich.edu/I-TASSER). Sequence alignments and homology modelings of Vps4 for Lokiarchaeota, Thorarchaeota, Heimdallarchaeota, and Odinarchaeota with unknown structures were carried out on MODELLER program(40), downloaded and installed from salilab server (https://salilab.org/modeller/download_installation.html). The three-dimensional structures of Vps2/24/46 and Vps20/32/60 for *S. cerevisiae* and four Asgard archaea were also built at the I-TASSER server. Among several three-dimensional models generated using homology modeling and ab initio method, the best model was selected after a series of refining and minimization and molecular dynamic simulation employing ff14SB force fields parameters by AMBER 16.0 package(41). Then the complexes of Vps2/24/46 and Vps20/32/60 against Vps4 were simulated using the ZDOCK server(42). Ten top docking poses were generated.

Molecular dynamic (MD) simulation

The parallel version of AMBER 16.0 package was used to prepare the complex files and conduct MD simulations employing ff14SB force fields parameters. The ionizable residues default protonation states in AMBER

16.0 were assigned. All MD simulations were carried out by applying cubic periodic boundary conditions (PBC) and in an explicit water box of TIP3P water molecules(43) with a minimum distance of 10.0 Å between complex surface and water box boundary. The Na^+ or Cl^- counterions were added in sufficient number to neutralize any net charges of the structures above. All of chemical bond lengths of hydrogen-heavy atoms were restrained by the SHAKE algorithm(44). A cutoff radius of 10.0 Å was set for both non-bonded electrostatic and van der Waals interactions. Long-range electrostatic forces were taken into account using Particle Mesh Ewald (PME) method(45). Langevin dynamics and Langevin piston methods were applied to keep the temperature (300 K) and the pressure (1 bar) of the system constant, respectively. The time step was set to 2.0 fs.

The solvated systems were minimized using PMEMD.CUDA module enabled NVIDIA graphics processing units (GPUs)(46, 47) in three stage, keeping the solute fixed and just minimized the positions of the water and counterions firstly with 100 kcal/(mol·$Å^2$) restraints and then reduced to 10 kcal/(mol·$Å^2$), and lastly for the entire system without any restraining force. Each stage was conducted with 10000 steps of steepest descent algorithm followed by 1000 steps conjugate gradient minimization to get rid of any unfavorable steric contacts for both solvent and protein molecules. Then, a

NVT simulation was conducted to slowly heat the systems temperature from 0 K to 300 K over a period of 500 ps, and density equilibrated for 2000 ps with a weak restraint applied to the whole protein at 1 atm and 300 K. Finally, all restraints were removed, and production MD simulations were carried out at constant pressure (1 atm) and temperature (300 K) in NPT ensemble. For each system, MD simulation was performed for 500 ns and repeated thrice with different random number, and a total of 1.5 μs trajectory was analyzed by CPPTRAJ module (48).

Calculations of binding free energy

The binding free energies of Vps2/24/46 and Vps20/32/60 against Vps4 were calculated by molecular mechanics-generalized Born surface area (MM-GBSA) method(28, 29). All energy components were calculated using 500 snapshots that were extracted every 200 ps during the last 100 ns of each MD simulation trajectory. The configurational entropy was not considered in the approach as it is extremely time-consuming. So the binding free energy in the solvent environment can be expressed as:

$$\Delta G_{\text{bind}} = \Delta E_{\text{ele}} + \Delta E_{\text{vdw}} + \Delta G_{\text{np}} + \Delta G_{\text{ele}}$$

The ΔE_{ele}, ΔE_{vdw}, ΔG_{np}, ΔG_{ele} represented electrostatic energy in the gas phase, Van der Waals energy in the gas phase, non-polar solvation energy, and polar solvation energy, respectively. All energy terms were calculated

439 using MM-GBSA calculations, and the ΔG_{ele} is estimated by GB model(29),
440 and the ΔG_{np} is calculated from the solvent accessible surface area (SASA)
441 of the molecules by molsurf, with the values 0.00542 and 0.92 for
442 SURFTEN and SURFOFF, respectively(49). The decomposition of binding
443 free energies were calculated at residue-pair level for a further investigation
444 of the complexes interactions using the MM-GBSA decomposition
445 program(50, 51) implemented in AMBER 16.0.

446 **Protein expression in *Escherichia coli* BL21 and purification for**
447 **biochemical assays *in vitro***

448 The Vps4, Vps2/24/46, and Vps20/32/60 coding sequences belonging to *S.*
449 *cerevisiae*, Lokiarchaeum_GC14_75, Thorarchaeota_AB_25,
450 Heimdallarchaeota_LC_3, and Odinarchaeota_LCB_4, and CdvC coding
451 sequences belonging to *Sulfolobus solfataricus*_P2, and Bathyarchaeota
452 from NCBI database (http://www.ncbi.nlm.nih.gov, accession number:
453 KZV07689.1, P36108.2, NP_013794.1; KKK42121.1, KKK42122.1,
454 KKK44605.1; OLS30569.1, OLS30568.1, OLS30800.1; OLS27542.1,
455 OLS27541.1, OLS27540.1; OLS18192.1, OLS18193.1, OLS18194.1,
456 AAK41192.1, WP_119819537.1, respectively) were codon optimized by
457 *GeneDesgin* (http://54.235.254.95/gd/) for expression in *E. coli* BL21,
458 synthesized (BGI Genomics Co., Ltd), and, respectively, cloned into a

pCold-TF vector (Takara Bio Co Ltd., Japan) that includes an N-terminal His tag and a soluble trigger factor chaperone tag. The *E. coli* BL21 (Takara Bio Co Ltd, Japan) beared the recombinant vectors were inoculated in LB medium containing 100 μg/ml carbenicillin, and incubated at 37°C until the OD_{600} reached at 0.6-0.8, and then the isopropyl-d-1-thiogalactopyranodside was added at the final concentration of 0.5 mM, followed by incubation at 15 °C for 18-24 h. The cells pellets were collected and resuspended in 20 ml binding buffer (20 mM phosphate buffer (pH 7.4), 500 mM NaCl, 50 mM imidazole, 1 mM dithiothreitol, 1 mM lysozyme, and 1 mM phenylmethylsulfonyl fluoride), followed by ultrasonic decomposition. Next, the target proteins were purified by Mag-Beads His-Tag Protein Purification Kit (BBI Co., Ltd, China) with wash buffer (20 mM phosphate buffer (pH 7.4), 500 mM NaCl, 100 mM imidazole, and 0.1% NP-40) and elution buffer (20 mM phosphate buffer (pH 7.4), 500 mM NaCl, and 500 mM imidazole). Finally, the purified proteins were concentrated to 1-2 ml in phosphate buffered saline (PBS, pH 7.4) by 30K Amicon Ultra-15 (Millipore Co Ltd., USA). Concentrations of these proteins were determined by Bradford Protein Assay Kit (Beytotime Bio Co Ltd., China). The purified Vps4, Vps2/24/46, and Vps20/32/60 belonging to *S. cerevisiae*, Lokiarchaeum_GC14_75, Thorarchaeota_AB_25,

Heimdallarchaeota_LC_3, and Odinarchaeota_LCB_4 were used for Isothermal titration calorimetry assay. The purified Vps4 belonging to *S. cerevisiae*, Lokiarchaeum_GC14_75, Thorarchaeota_AB_25, Heimdallarchaeota_LC_3, and Odinarchaeota_LCB_4, and Cdv belonging to *Sulfolobus solfataricus*_P2, and Bathyarchaeota were used for ATPase activity assay.

Isothermal titration calorimetry assay

Isothermal titration calorimetry assay (ITC) was carried out at 25°C using an ITC200 system (MicroCal, USA). The Vps4 MIT domain (3 μM in PBS buffer) was placed in cell and titrated with 19 injections of 10 μl of Vps2/24/46 or Vps20/32/60 (33 μM in PBS buffer) at 2 min intervals. The heat of ligand dilution into buffer was subtracted from the reaction heat, after removing the data of 1st injection. Data analysis was carried out using Origin 7.0 (MicroCal, USA).

ATPase activity assay

The ATPase activity was determined by a slightly modified malachite green assay(52). In short, the purified proteins (4 μM) were incubated with reaction buffer (1 mM ATP, 20 mM HEPES pH 7.4, 100 mM NaCl, 10 mM $MgCl_2$, 1 mM DTT) in a total volume of 50 μl at the indicated temperature for 90 min, and was immediately stopped by liquid nitrogen. Then, the

499 reaction mixture was added with 100 μl of malachite green color buffer (14
500 mM ammonium molybdate, 1.3 M HCl, and 1.5 mM malachite green) and
501 50 μl of 21% (w/v) citric acid, followed by incubation at room temperature
502 for 30 min. Finally, the reaction mixture that turned green was attributed to
503 the free phosphate released by Vps4 ATP hydrolysis. Additionally, the
504 control experiments were identical to the treatment group, except that the
505 mixture of Vps4 and reaction buffer was immediately treated with liquid
506 nitroge before addition of malachite green color buffer and citric acid; and
507 these experiments were to eliminate the interference of irrelevant free
508 phosphate. Also, the empty vector was served to prove that the ATP
509 hydrolysis is due to Vps4.

510 **_S. cerevisiae_ strains and cultivation**

511 The *S. cerevisiae* strain BY4741 (*MATa leu2Δ0 met15Δ0 ura3Δ0 his3Δ1*)
512 and its derivative *vps4* null mutant strain YPR173Ca (designated the *S.*
513 *cerevisiae*Δ*vps4* in this study) were from *S. cerevisiae* deletion mutant
514 library (53). *S. cerevisiae* cells were routinely cultured in YPD medium (10
515 g/L yeast extract, 20 g/L peptone, 20 g/L glucose) or SC-Ura medium (6.7
516 g/L YNB, 0.01μmol/L $Fe(NH_4)_2(SO_4)_2$, 20 g/L glucose, and complete amino
517 acids without uracil) at 30 ºC unless otherwise noted. The solid media were
518 identical to those of YPD or SC-Ura except that agar was present.

Complementation Assay

The Vps4 coding sequences belonging to Lokiarchaeum_GC14_75, Thorarchaeota_AB_25, Heimdallarchaeota_LC_3, and Odinarchaeota_LCB_4, and CdvC coding sequences belonging to *Sulfolobus solfataricus*_P2, and Bathyarchaeota (NCBI accession number: KKK42121.1, OLS30569.1, OLS27542.1, OLS18192.1, AAK41192.1, WP_119819537.1, respectively) were codon optimized by *GeneDesgin* (http://54.235.254.95/gd/) for expression in *S. cerevisiae*, before synthesis by BGI Genomics Co., Ltd (54). To eliminate the interference of transcriptional level factor, a native promoter region of *S. cerevisiae* BY4741 *vps4* (a 500 bp DNA sequence region upstream from the ATG start codon of this gene) was used to drive the coding sequences. Then, we assembled the coding sequences, the *S. cerevisiae vps4* native promoter, and a *S. cerevisiae* CYC1 (Cytochrome c isoform 1) terminator into a pPOT-RFP vector according to a developed YeastFab Assembly protocol(31). Besides, the pPOT-RFP vector containing the entire *S. cerevisiae* BY4741 *vps4* with its native promoter and the CYC1 terminator were transformed into the *vps4* null mutant *S. cerevisiae*(32), and this reconstituted strain was designated the "+*S. cerevisiae*". In this study, both the *S. cerevisiae* and *S. cerevisiae vps4Δ* were transformed with the pPOT-RFP vector as the control.

FM-64M staining

S. cerevisiae cells of each strain were cultured in SC-Ura medium at 30 ºC and normalized to an OD_{600} of 0.5-0.8. Then, the *S. cerevisiae* cells were stained with 80 μM FM-64M (AAT Bioquest Co Ltd., China) at 30 ºC for 20 min, and next cultured for 120 min after washes with medium. Finally, the *S. cerevisiae* cells were examined under a N-STORM fluorescence microscope (Nikon Co Ltd., Japan).

ACKNOWLEDGMENT

This work was supported by the National Natural Science Foundation of China (Grant Nos. 91851105, 31622002, 31970105, 31725002, 21625302, 31800615), the China Postdoctoral Science Foundation (Grant No. 2018M643153), the Basic and Applied Basic Research of Guangdong Province (Grant No. 2019A1515110089), the Shenzhen Science and Technology Program (Grant No. JCYJ20170818091727570, KQTD20180412181334790), Shenzhen Key Laboratory of Synthetic Genomics (ZDSYS201802061806209), Guangdong Provincial Key Laboratory of Synthetic Genomics (2019B030301006) and the Key Project of Department of Education of Guangdong Province (No. 2017KZDXM071). EVK is supported by the Intramural Research Program funds of the National Institutes of Health of the USA.

AUTHOR' CONTRIBUTIONS

Zhongyi Lu and Meng Li conceived and designed the experiments. Zhongyi Lu, Tianyi Li, Siyu Zhang, and Jinquan Li performed the experiments. Huiying Chu and Guohui Li designed the molecular dynamics strategy. Ting Fu performed the simulations. Zhongyi Lu, Ting Fu, and Huiying Chu analyzed the data. Yang Liu and Junbiao Dai contributed reagents/materials/analysis tools. Zhongyi Lu, Ting Fu, Eugene Koonin and Meng Li wrote and all authors edited and approved the paper.

CONFLICT OF INTEREST

The authors declare no conflict of interest.

REFERENCE

1. Dacks JB, Peden AA, Field MC. 2009. Evolution of specificity in the eukaryotic endomembrane system. Int J Biochem Cell Biol 41:330-40.
2. Hartman H, Fedorov A. 2002. The origin of the eukaryotic cell: a genomic investigation. Proc Natl Acad Sci U S A 99:1420-5.
3. Babst M, Sato TK, Banta LM, Emr SD. 1997. Endosomal transport function in yeast requires a novel AAA-type ATPase, Vps4p. EMBO J 16:1820-31.
4. Bowers K, Lottridge J, Helliwell SB, Goldthwaite LM, Luzio JP, Stevens TH. 2004. Protein-protein interactions of ESCRT complexes in the yeast Saccharomyces cerevisiae. Traffic 5:194-210.
5. Olmos Y, Carlton JG. 2016. The ESCRT machinery: new roles at new holes. Curr Opin Cell Biol 38:1-11.
6. McCullough J, Frost A, Sundquist WI. 2018. Structures, Functions, and Dynamics of ESCRT-III/Vps4 Membrane Remodeling and Fission Complexes. Annu Rev

Cell Dev Biol doi:10.1146/annurev-cellbio-100616-060600.

7. Leung KF, Dacks JB, Field MC. 2008. Evolution of the multivesicular body ESCRT machinery; retention across the eukaryotic lineage. Traffic 9:1698-716.

8. Wollert T, Wunder C, Lippincott-Schwartz J, Hurley JH. 2009. Membrane scission by the ESCRT-III complex. Nature 458:172-7.

9. Obita T, Saksena S, Ghazi-Tabatabai S, Gill DJ, Perisic O, Emr SD, Williams RL. 2007. Structural basis for selective recognition of ESCRT-III by the AAA ATPase Vps4. Nature 449:735-9.

10. Kieffer C, Skalicky JJ, Morita E, De Domenico I, Ward DM, Kaplan J, Sundquist WI. 2008. Two distinct modes of ESCRT-III recognition are required for VPS4 functions in lysosomal protein targeting and HIV-1 budding. Dev Cell 15:62-73.

11. Kojima R, Obita T, Onoue K, Mizuguchi M. 2016. Structural Fine-Tuning of MIT-Interacting Motif 2 (MIM2) and Allosteric Regulation of ESCRT-III by Vps4 in Yeast. J Mol Biol 428:2392-2404.

12. Caspi Y, Dekker C. 2018. Dividing the Archaeal Way: The Ancient Cdv Cell-Division Machinery. Front Microbiol 9:174.

13. Makarova KS, Yutin N, Bell SD, Koonin EV. 2010. Evolution of diverse cell division and vesicle formation systems in Archaea. Nat Rev Microbiol 8:731-41.

14. Samson RY, Obita T, Hodgson B, Shaw MK, Chong PL, Williams RL, Bell SD. 2011. Molecular and structural basis of ESCRT-III recruitment to membranes during archaeal cell division. Mol Cell 41:186-96.

15. Lindas AC, Karlsson EA, Lindgren MT, Ettema TJ, Bernander R. 2008. A unique cell division machinery in the Archaea. Proc Natl Acad Sci U S A 105:18942-6.

16. Samson RY, Dobro MJ, Jensen GJ, Bell SD. 2017. The Structure, Function and Roles of the Archaeal ESCRT Apparatus. Subcell Biochem 84:357-377.

17. Liu J, Gao R, Li C, Ni J, Yang Z, Zhang Q, Chen H, Shen Y. 2017. Functional assignment of multiple ESCRT-III homologs in cell division and budding in Sulfolobus islandicus. Mol Microbiol 105:540-553.

18. Spang A, Saw JH, Jorgensen SL, Zaremba-Niedzwiedzka K, Martijn J, Lind AE, van Eijk R, Schleper C, Guy L, Ettema TJG. 2015. Complex archaea that bridge the gap between prokaryotes and eukaryotes. Nature 521:173-179.

19. Zaremba-Niedzwiedzka K, Caceres EF, Saw JH, Backstrom D, Juzokaite L, Vancaester E, Seitz KW, Anantharaman K, Starnawski P, Kjeldsen KU, Stott MB, Nunoura T, Banfield JF, Schramm A, Baker BJ, Spang A, Ettema TJ. 2017. Asgard archaea illuminate the origin of eukaryotic cellular complexity. Nature 541:353-358.

20. Seitz KW, Dombrowski N, Eme L, Spang A, Lombard J, Sieber JR, Teske AP, Ettema TJG, Baker BJ. 2019. Asgard archaea capable of anaerobic hydrocarbon cycling. Nat Commun 10:1822.

21. Liu Y, Zhou Z, Pan J, Baker BJ, Gu JD, Li M. 2018. Comparative genomic inference suggests mixotrophic lifestyle for Thorarchaeota. ISME J 12:1021-1031.

22. Imachi H, Nobu MK, Nakahara N, Morono Y, Ogawara M, Takaki Y, Takano Y, Uematsu K, Ikuta T, Ito M, Matsui Y, Miyazaki M, Murata K, Saito Y, Sakai S, Song C, Tasumi E, Yamanaka Y, Yamaguchi T, Kamagata Y, Tamaki H, Takai K. 2019. Isolation of an archaeon at the prokaryote-eukaryote interface. Nature doi:

10.1038/s41586-019-1916-6.

23. Monroe N, Hill CP. 2016. Meiotic Clade AAA ATPases: Protein Polymer Disassembly Machines. J Mol Biol 428:1897-911.
24. Gonciarz MD, Whitby FG, Eckert DM, Kieffer C, Heroux A, Sundquist WI, Hill CP. 2008. Biochemical and structural studies of yeast Vps4 oligomerization. J Mol Biol 384:878-95.
25. Yang B, Stjepanovic G, Shen Q, Martin A, Hurley JH. 2015. Vps4 disassembles an ESCRT-III filament by global unfolding and processive translocation. Nat Struct Mol Biol 22:492-8.
26. Da Cunha V, Gaia M, Nasir A, Forterre P. 2018. Asgard archaea do not close the debate about the universal tree of life topology. PLoS Genet 14:e1007215.
27. Spang A, Stairs CW, Dombrowski N, Eme L, Lombard J, Caceres EF, Greening C, Baker BJ, Ettema TJG. 2019. Proposal of the reverse flow model for the origin of the eukaryotic cell based on comparative analyses of Asgard archaeal metabolism. Nat Microbiol 4:1138-1148.
28. Kollman PA, Massova I, Reyes C, Kuhn B, Huo S, Chong L, Lee M, Lee T, Duan Y, Wang W, Donini O, Cieplak P, Srinivasan J, Case DA, Cheatham TE, 3rd. 2000. Calculating structures and free energies of complex molecules: combining molecular mechanics and continuum models. Acc Chem Res 33:889-97.
29. Bashford D, Case DA. 2000. Generalized born models of macromolecular solvation effects. Annual Review of Physical Chemistry 51:129-152.
30. Stuchell-Brereton MD, Skalicky JJ, Kieffer C, Karren MA, Ghaffarian S, Sundquist WI. 2007. ESCRT-III recognition by VPS4 ATPases. Nature 449:740-4.
31. Guo Y, Dong J, Zhou T, Auxillos J, Li T, Zhang W, Wang L, Shen Y, Luo Y, Zheng Y, Lin J, Chen GQ, Wu Q, Cai Y, Dai J. 2015. YeastFab: the design and construction of standard biological parts for metabolic engineering in Saccharomyces cerevisiae. Nucleic Acids Res 43:e88.
32. Gietz RD, Schiestl RH. 2007. Quick and easy yeast transformation using the LiAc/SS carrier DNA/PEG method. Nat Protoc 2:35-7.
33. Scheuring S, Rohricht RA, Schoning-Burkhardt B, Beyer A, Muller S, Abts HF, Kohrer K. 2001. Mammalian cells express two VPS4 proteins both of which are involved in intracellular protein trafficking. J Mol Biol 312:469-80.
34. Scheuring S, Bodor O, Rohricht RA, Muller S, Beyer A, Kohrer K. 1999. Cloning, characterisation, and functional expression of the Mus musculus SKD1 gene in yeast demonstrates that the mouse SKD1 and the yeast VPS4 genes are orthologues and involved in intracellular protein trafficking. Gene 234:149-59.
35. Mount DW. 2007. Using the basic local alignment search tool (BLAST). Cold Spring Harbor Protocols 2007:pdb. top17.
36. Edgar RC. 2004. MUSCLE: a multiple sequence alignment method with reduced time and space complexity. BMC Bioinformatics 5:113.
37. Capella-Gutierrez S, Silla-Martinez JM, Gabaldon T. 2009. trimAl: a tool for automated alignment trimming in large-scale phylogenetic analyses. Bioinformatics 25:1972-3.
38. Nguyen LT, Schmidt HA, von Haeseler A, Minh BQ. 2015. IQ-TREE: a fast and effective stochastic algorithm for estimating maximum-likelihood phylogenies. Mol Biol Evol 32:268-74.

678 39. Sun S, Li L, Yang F, Wang X, Fan F, Yang M, Chen C, Li X, Wang HW, Sui SF.
679 2017. Cryo-EM structures of the ATP-bound Vps4(E233Q) hexamer and its
680 complex with Vta1 at near-atomic resolution. Nat Commun 8:16064.
681 40. Sanchez R, Sali A. 2000. Comparative protein structure modeling. Introduction
682 and practical examples with modeller. Methods Mol Biol 143:97-129.
683 41. D.A. Case RMB, D.S. Cerutti, T.E. Cheatham, III, T.A. Darden, R.E. Duke, T.J.
684 Giese, H. Gohlke,, A.W. Goetz NH, S. Izadi, P. Janowski, J. Kaus, A. Kovalenko,
685 T.S. Lee, S. LeGrand, P. Li, C., Lin TL, R. Luo, B. Madej, D. Mermelstein, K.M.
686 Merz, G. Monard, H. Nguyen, H.T. Nguyen, I., Omelyan AO, D.R. Roe, A.
687 Roitberg, C. Sagui, C.L. Simmerling, W.M. Botello-Smith, J. Swails,, R.C.
688 Walker JW, R.M. Wolf, X. Wu, L. Xiao and P.A. Kollman. 2016. AMBER 2016,
689 University of California, San Francisco.
690 42. Pierce BG, Wiehe K, Hwang H, Kim BH, Vreven T, Weng Z. 2014. ZDOCK
691 server: interactive docking prediction of protein-protein complexes and symmetric
692 multimers. Bioinformatics 30:1771-3.
693 43. Jorgensen WL, Chandrasekhar J, Madura JD, Impey RW, Klein ML. 1983.
694 Comparison of Simple Potential Functions for Simulating Liquid Water. Journal
695 of Chemical Physics 79:926-935.
696 44. Ryckaert JP, Ciccotti G, Berendsen HJC. 1977. Numerical-Integration of
697 Cartesian Equations of Motion of a System with Constraints - Molecular-
698 Dynamics of N-Alkanes. Journal of Computational Physics 23:327-341.
699 45. Essmann U, Perera L, Berkowitz ML, Darden T, Lee H, Pedersen LG. 1995. A
700 Smooth Particle Mesh Ewald Method. Journal of Chemical Physics 103:8577-
701 8593.
702 46. Gotz AW, Williamson MJ, Xu D, Poole D, Le Grand S, Walker RC. 2012. Routine
703 Microsecond Molecular Dynamics Simulations with AMBER on GPUs. 1.
704 Generalized Born. J Chem Theory Comput 8:1542-1555.
705 47. Salomon-Ferrer R, Gotz AW, Poole D, Le Grand S, Walker RC. 2013. Routine
706 Microsecond Molecular Dynamics Simulations with AMBER on GPUs. 2.
707 Explicit Solvent Particle Mesh Ewald. J Chem Theory Comput 9:3878-88.
708 48. Roe DR, Cheatham TE, 3rd. 2013. PTRAJ and CPPTRAJ: Software for
709 Processing and Analysis of Molecular Dynamics Trajectory Data. J Chem Theory
710 Comput 9:3084-95.
711 49. Weiser J, Shenkin PS, Still WC. 1999. Approximate atomic surfaces from linear
712 combinations of pairwise overlaps (LCPO). Journal of Computational Chemistry
713 20:217-230.
714 50. Tsui V, Case DA. 2001. Theory and applications of the generalized Born solvation
715 model in macromolecular Simulations. Biopolymers 56:275-291.
716 51. Wang W, Donini O, Reyes CM, Kollman PA. 2001. Biomolecular simulations:
717 Recent developments in force fields, simulations of enzyme catalysis, protein-
718 ligand, protein-protein, and protein-nucleic acid noncovalent interactions. Annual
719 Review of Biophysics and Biomolecular Structure 30:211-243.
720 52. Merrill SA, Hanson PI. 2010. Activation of human VPS4A by ESCRT-III proteins
721 reveals ability of substrates to relieve enzyme autoinhibition. J Biol Chem
722 285:35428-38.
723 53. Giaever G, Chu AM, Ni L, Connelly C, Riles L, Veronneau S, Dow S, Lucau-

Danila A, Anderson K, Andre B, Arkin AP, Astromoff A, El-Bakkoury M, Bangham R, Benito R, Brachat S, Campanaro S, Curtiss M, Davis K, Deutschbauer A, Entian KD, Flaherty P, Foury F, Garfinkel DJ, Gerstein M, Gotte D, Guldener U, Hegemann JH, Hempel S, Herman Z, Jaramillo DF, Kelly DE, Kelly SL, Kotter P, LaBonte D, Lamb DC, Lan N, Liang H, Liao H, Liu L, Luo C, Lussier M, Mao R, Menard P, Ooi SL, Revuelta JL, Roberts CJ, Rose M, Ross-Macdonald P, Scherens B, et al. 2002. Functional profiling of the Saccharomyces cerevisiae genome. Nature 418:387-91.

54. Richardson SM, Wheelan SJ, Yarrington RM, Boeke JD. 2006. GeneDesign: rapid, automated design of multikilobase synthetic genes. Genome Res 16:550-6.

Figures Legends

FIG 1. Phylogenetic and amino acid sequence analysis of the ESCRT-III-related subunits in archaea and eukarya. (A) Unrooted maximum-likelihood phylogenetic tree of the ESCRT-III-related subunits in archaea and eukarya. The information of the Asgard Vps2/24/46 and Vps20/32/60 can be found in Table S1. Part of the bootstrap values are shown on nodes. (B) Predicted MIM1 and MIM2 in Asgard Vps2/24/46 and Vps20/32/60, respectively. The information of proteins used here can be found in Table S1. The ESCRT-III core domain, C-terminal helix, and MIM1 and MIM2 are presented.

FIG 2. Phylogenetic and structural analysis of the Asgard Vps4.

(A) Unrooted maximum likelihood phylogenetic analysis of the Vps4-related in archaea and eukarya. The information of the Asgard Vps4 can be found in Table S1. Part of the bootstrap values are shown on nodes. (B)

751 Phylogenetic (a) and structural (b) analysis of the Asgard Vps4 MIT domain.
752 The sequences of CdvC MIT domain are used as the outgroup to further
753 confirm the phylogenetic relationship of the MIT domain in eukaryotic and
754 Asgard Vps4. The antiparallel three-helix bundle of MIT domains is shown
755 explicitly.

756

757 **FIG 3. Comparison of the Vps4 (surface representation, grey) in**
758 **complex with ESCRT-III subunits (ribbon representation, blue) in**
759 **Asgard archaea.**

760 The MIM1 and MIM2 are shown in orange (stick representation, orange)
761 and highlighted in red in close-up views (space filling representation). The
762 black letters indicated main residues in MIT domains that contribute to the
763 interaction. The Vps4 MIT domain in complex with (A) Vps2/24/46 and (B)
764 Vps20/32/60 subunits in *S. cerevisiae*, Heimdall_LC_3, Odin_LCB_4,
765 Thor_AB_25, and Loki_GC14_75 are indicated.

766

767 **FIG 4. Functional complementation of *Saccharomyces cerevisiae* vps4**
768 **null mutants by Asgard Vps4.**

769 (A) Complementation of the high-temperature-sensitive growth defect of
770 vps4 mutant cells. Five microliters of a series of 10-fold dilutions derived

from a starting suspension of an OD_{600} of 10^{-1} was inoculated into SC-Ura medium. (B) The ATPase activity of *S. cerevisiae* Vps4, Asgard Vps4 and Cdvs at 30 ºC and 39 ºC were, respectively, confirmed by a malachite green assay. The substrates would turn from golden to green owing to the inorganic phosphate relased form ATP hydrolysis by Vps4 under the indicated condition. (C) The class E compartments in *S. cerevisiae* vps4 null mutants were largely abrogated by Asgard Vps4. The vacuolar morphologies in the indicated strains were visualized by fluorescent microscopy. Arrowhead highlights the class E compartment in vps4 null mutant. Scale bar=10 μm. Quantification of class E compartment in the indicated strains. The results represented the means from three independent replicates (20 cells per experiment), and standard deviations are indicated with error bars. Statistical significance was assessed by one-way analysis of variance with Bonferroni's multiple-comparison test. **, $P<0.01$.

Supplemental information

FIG S1. Phylogenetic analysis of ESCRT-III-related proteins in the eukarya and archaea. The tree was reconstructed by maximum likelihood analysis using 156 representative amino acid sequences based on LG+G4 model (recommended by the "TESTONLY"), with option "-bb 1000", and the bootstrap values are shown on nodes.

FIG S2. Phylogenetic analysis of Vps4-related proteins in eukarya and archaea. The tree was reconstructed by maximum likelihood analysis using 76 representative amino acid sequences based on LG+I+G4 model (recommended by the "TESTONLY"), with option "-bb 1000", and the bootstrap values are shown on nodes.

FIG S3. Predicted "arginine collar" in Vps4 of Asgard archaea and eukarya. (A) The Walker A, Walker B, Sensor I, ARG finger, and Sensor II are conserved across all the indiactaed sequences, and are shown to confirm the location of "arginine collar". Conserved arginine residues of "arginine collar" are highlighted (red shading and red letters, respectively). The information of proteins used here can be found in Table S1. (B) The top and bottom views of the hexameric ring (grey) were constructed by

Heimdall_LC_3 Vps4 (white) as the example to demonstrate the location of "arginine collar", including R222, R231, and R232.

FIG S4. Phylogenetic analysis of the Microtubule Interacting and Transport domain in Vps4-related proteins. The tree was reconstructed by maximum likelihood analysis using 48 amino acid sequences based on LG+I+G4 model (recommended by the "TESTONLY"), with option "-bb 1000", and the bootstrap values are shown on nodes.

FIG S5. The number of Vps4 and CdvC Microtubule Interacting and Transport domain amino acid residues in alpha conformation of Asgard archaea, *Saccharomyces cerevisiae* and TACK archaea during molecular dynamic simulations. The curves of the numbers of Vps4 MIT domain amino acid residues in alpha conformation of Asgard and *S. cerevisiae*, which were calculated from the last 200 ns MD simulation trajectories, were plotted against simulation time.

FIG S6. ITC binding profiles of Asgard Vps4 Microtubule Interacting and Transport domain titrated with Asgard Vps2/24/46 and Vps20/32/60. (A) The curve of Heimdall_LC_3 TF-Vps4-MIT titrated with

Heimdall_LC_3 TF-Vps2/24/46 was fit to Sequential Binding Sites; ΔH_1=-4.73×10^5 cal mol^{-1}; ΔH_2=9.31×10^5 cal mol^{-1}. The curve of Heimdall_LC_3-Vps4-MIT titrated with Heimdall_LC_3 TF-Vps20/32/60 was fit to Sequential Binding Sites; ΔH_1=2.78×10^6 cal mol^{-1}; ΔH_2=-2.31×10^6 cal mol^{-1}. (B) The curve of Odin_LCB_4 TF-Vps4-MIT titrated with Odin_LCB_4 Vps2/24/46 was fit to One Set of Sites; ΔH=3.92×10^5 cal mol^{-1}. The curve of Odin_LCB_4 TF-Vps4-MIT titrated with Odin_LCB_4 TF-Vps20/32/60 was fit to One Set of Sites; ΔH=3.31×10^5 cal mol^{-1}. (C) The curve of Thor_AB_25 TF-Vps4-MIT titrated with Thor_AB_25 TF-Vps2/24/46 was fit Sequential Binding Sites; ΔH_1=3.25×10^8 cal mol^{-1}; ΔH_2=1.29×10^6 cal mol^{-1}. The curve of Thor_AB_25 TF-Vps4-MIT titrated with Thor_AB_25 TF-Vps20/32/60 was fit to One Set of Sites; ΔH=1.62×10^6 cal mol^{-1}. (D) The curve of Loki_GC14_75 TF-Vps4-MIT titrated with Loki_GC14_75 TF-Vps2/24/46 was fit to Sequential Binding Sites; ΔH_1=-1.21×10^5 cal mol^{-1}; ΔH_2=4.22×10^5 cal mol^{-1}. The curve of Loki_GC14_75 TF-Vps4-MIT titrated with Loki_GC14_75 TF-Vps20/32/60 was fit to One Set of Sites; ΔH=1.42×10^6 cal mol^{-1}. Binding to a TF control surface was negligible (not shown).

TABLE S1. Summary of proteins used in this study.

TABLE S2. The predicted binding free energies between Vps4 and ESCRT-III subunits (Vps2/24/46 (A), and Vps20/32/60 (B)).

TABLE S3. The dominant amino acid residues of Vps4 Microtubule Interacting and Transport domain involved in binding with Vps2/24/46 are listed.

TABLE S4. The dominant amino acid residues of Vps4 Microtubule Interacting and Transport domain involved in binding with Vps20/32/60 are listed.

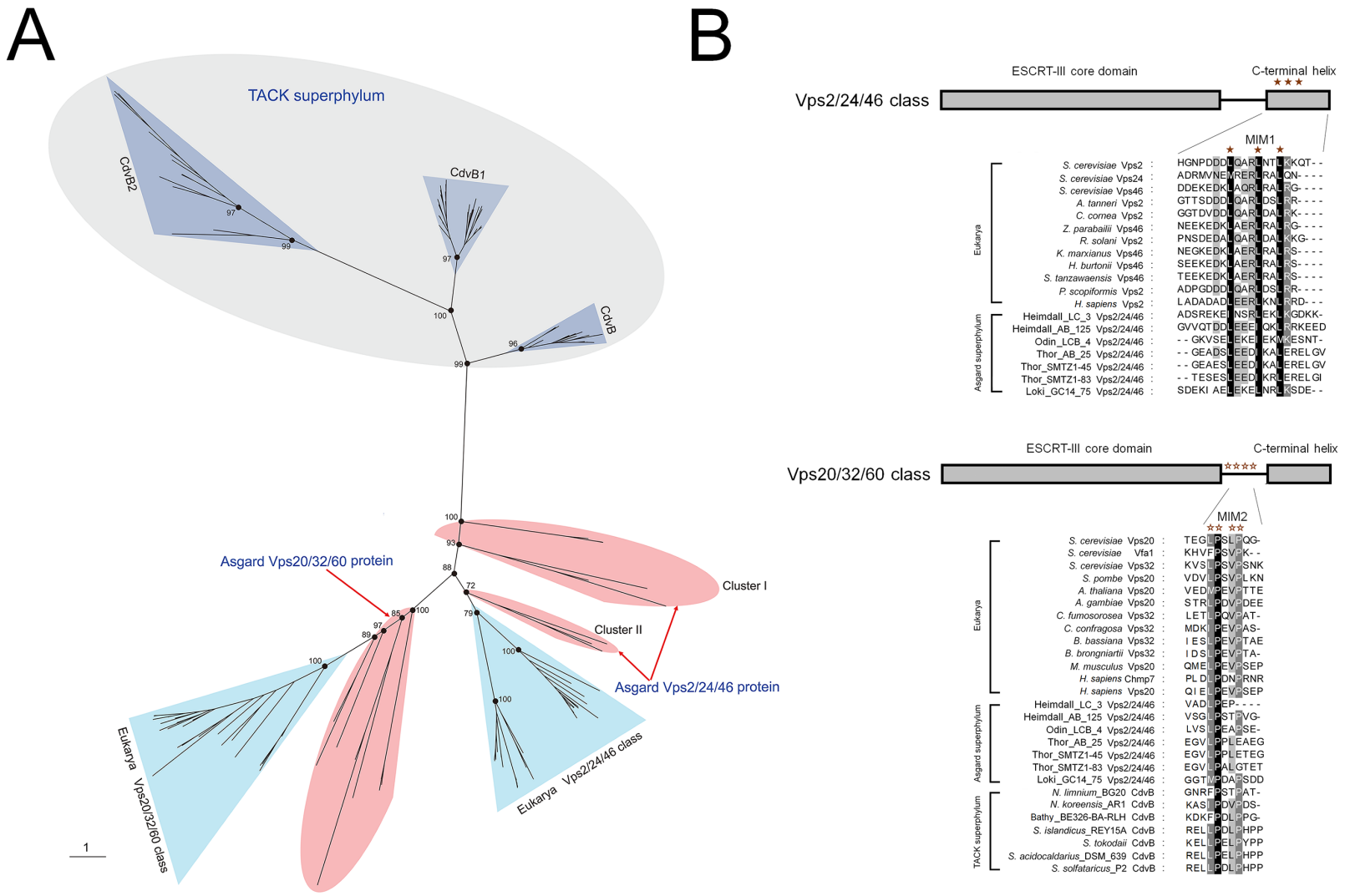

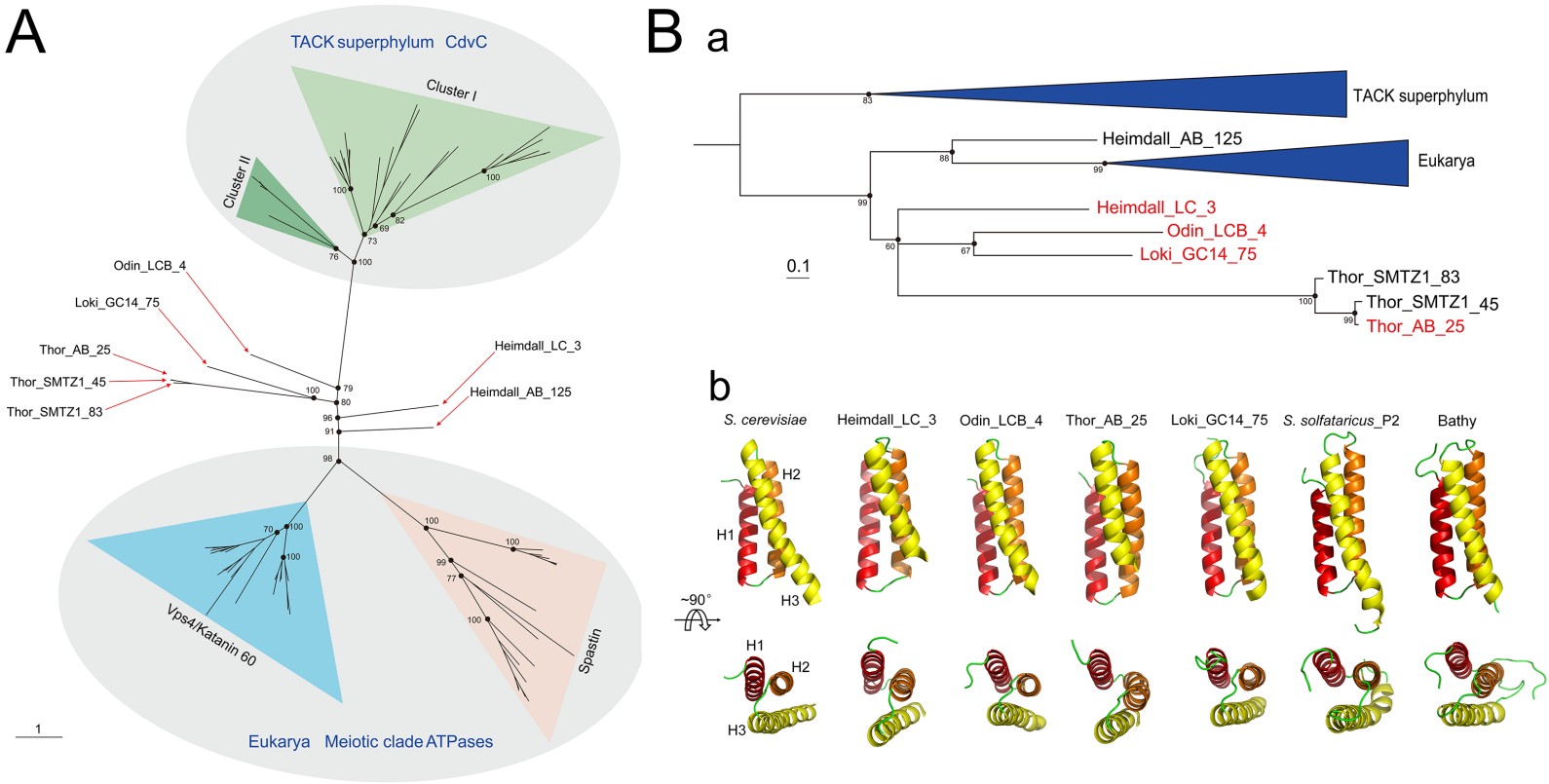

A

S. cerevisiae

Vps4 MIT vs Vps2

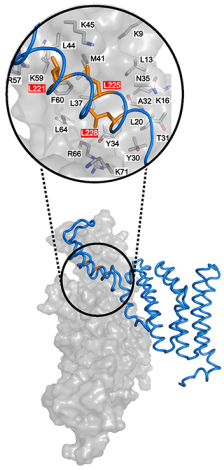

Heimdall_LC_3

Vps4 MIT vs Vps2/24/46

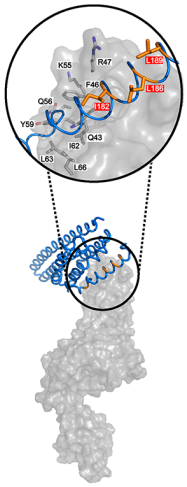

Odin_LCB_4

Vps4 MIT vs Vps2/24/46

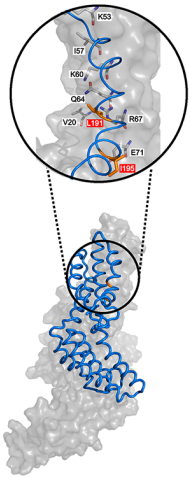

Thor_AB_25

Vps4 MIT vs Vps2/24/46

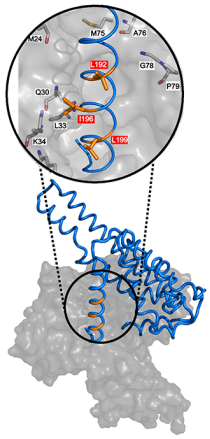

Loki_GC14_75

Vps4 MIT vs Vps2/24/46

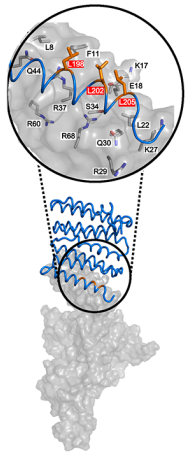

B

Vps4 MIT vs Vps20

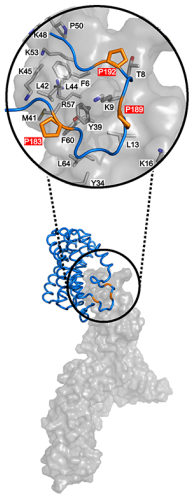

Vps4 MIT vs Vps20/32/60

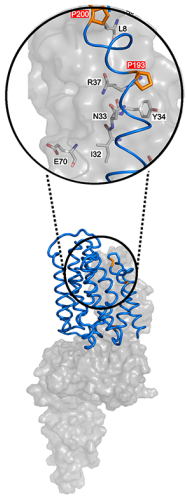

Vps4 MIT vs Vps20/32/60

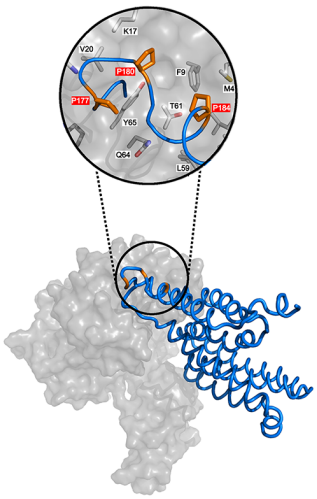

Vps4 MIT vs Vps20/32/60

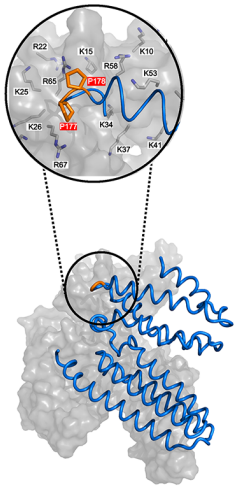

Vps4 MIT vs Vps20/32/60